

Effect of tangential swirl air inlet angle on the combustion efficiency of a hybrid powder-solid ramjet]

Xu, Y., Jia, R., Medina, H. & Sun, H.

Author post-print (accepted) deposited by Coventry University's Repository

Original citation & hyperlink:

Xu, Y, Jia, R, Medina, H & Sun, H 2019, 'Effect of tangential swirl air inlet angle on the combustion efficiency of a hybrid powder-solid ramjet', *Acta Astronautica*, vol. 159, pp. 87-95.

<https://dx.doi.org/10.1016/j.actaastro.2019.03.046>

DOI 10.1016/j.actaastro.2019.03.046

ISSN 0094-5765

Publisher: Elsevier

NOTICE: this is the author's version of a work that was accepted for publication in *Acta Astronautica*. Changes resulting from the publishing process, such as peer review, editing, corrections, structural formatting, and other quality control mechanisms may not be reflected in this document. Changes may have been made to this work since it was submitted for publication. A definitive version was subsequently published in *Acta Astronautica*, [159], (2019) DOI: 10.1016/j.actaastro.2019.03.046

© 2019, Elsevier. Licensed under the Creative Commons Attribution-NonCommercial-NoDerivatives 4.0 International

<http://creativecommons.org/licenses/by-nc-nd/4.0/>

Copyright © and Moral Rights are retained by the author(s) and/ or other copyright owners. A copy can be downloaded for personal non-commercial research or study, without prior permission or charge. This item cannot be reproduced or quoted extensively from without first obtaining permission in writing from the copyright holder(s). The content must not be changed in any way or sold commercially in any format or medium without the formal permission of the copyright holders.

This document is the author's post-print version, incorporating any revisions agreed during the peer-review process. Some differences between the published version and this version may remain and you are advised to consult the published version if you wish to cite from it.

Effect of tangential swirl air inlet angle on the combustion efficiency of a hybrid powder-solid ramjet

Yihua Xu^(a), Rui Jia^(a), Humberto Medina^(b), Haijun Sun^(a)

(a) School of Aircraft Engineering, Nanchang Hangkong University, Nanchang, Jiangxi, 330063, PR China

(b) School of Mechanical, Aerospace and Automotive Engineering, Coventry University, Coventry, CV1 5FB, UK

Abstract: A new ramjet configuration using powder and solid fuel as propellant is investigated, namely, hybrid powder-solid ramjet (HPSR). Boron particles were used as the powder in this study. In order to improve combustion efficiency of boron and simplify the engine structure, a tangential swirl air inlet is adopted on the HPSR. Ignition model based on the multi-layer oxide structure and Global reaction combustion model of boron particles, the Lagrangian particle trajectory model and the realizable k- ϵ turbulence model were implemented to calculate three-dimensional two-phase flow and combustion in the HPSR with the different tangential air inlet angles ($0^\circ, 5^\circ, 10^\circ, 15^\circ, 20^\circ, 25^\circ$). The effects of tangential air inlet angles on the ignition and combustion of boron were analyzed. The results show that when the tangential swirl air inlet angle is 10° , the combustion efficiency of boron particles and the total combustion efficiency of engine are the highest; the temperature distribution in the second combustion chamber is uniform, and the ignition distance of particles is small, for the HPSR configuration tested.

Key words: HPSR; swirl; tangential air inlet angle; Boron; ignition and combustion; ramjet

1. Introduction

High energy propellants with metallic particles have been applied in solid ramjet[1]-[5] on a large-scale. However, the content of metal powder is seriously limited to the propellant processing technique[6][8] and it is difficult to regulate the thrust of the engine for the solid ramjet[9][10]. In order to improve engine specific impulse and its maneuverability, the powder ramjet engine was proposed[11][15]. Although the fuel flow rate of the powder ramjet is easy to adjust for improving maneuverability, and the specific impulse is high because of the high energy contained in metal powder, it is difficult to achieve a self-sustaining burn of pure metal powder because a high temperature environment is required for metal powder combustion. Therefore, in order to make use of the easy-to-adjust characteristics of powder flow rate, combined with the high temperature environment of solid ramjets, a hybrid powder-solid ramjet (HPSR) is investigated here.

A HPSR (as shown in Figure 1), not like the hybrid rocket engine[16][17], consists of the following main components: a combustion gas generator, a powder injector, an air inlet, a second combustion chamber and a nozzle. The solid powder is sprayed from the head of the second combustion chamber and a larger number of solid particles are burned in the combustion chamber to increase the working temperature and total pressure, which results in improved engine performance. There are many similarities in both the structural design and the working principle between a solid ramjet and a HPSR. Combustion gas coming from the generator and metal powder fuel enter the combustion chamber mix with ramming air which combusts to produce gas at high temperature. This gas is discharged at the engine nozzle to produce thrust. The key difference between them is that in a solid rocket ramjet oxygen deficient propellant contains the metal particles as additive fuel and metal particles in the HPSR are

injected by a powder injector. This injection allows the adjustment of the powder flow rate.

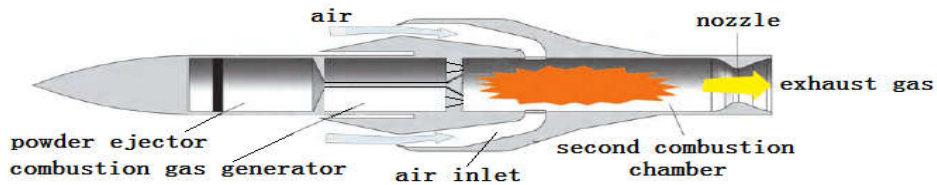


Figure 1 Hybrid powder-solid ramjet sketch

Among the choices of metal powders that can be used, such as aluminum, magnesium, boron, etc. Boron has higher volume and mass calorific values. Furthermore, in a high temperature engine environment, the combustion product of boron is gas phase rather than condensate phase because the boiling temperature of B_2O_3 is 2316K, which will not cause the loss of thrust. Therefore, boron has become the first choice for people to study the powder-based ramjet used for air-breathing missiles.

Solid ramjets using boron have been widely studied[18]-[23]. For example, T. dawara, et al. [18] measured ignition delay time of boron particles and analyzed the ignition and combustion characteristics of boron containing gas generators by direct-connect tests. A. Gany[19] investigated the characteristics of boron combustion in air-breathing propulsion, and found that the unfavorable thermochemical equilibrium results in energy trapping and loss of potential chemical energy, and a specific thermodynamic blocking effect, which can cause incomplete reaction in actual boron-loaded systems basing on the peculiar ignition phenomena of individual boron particles and the specific conditions required to sustain combustion. B. Chen, et al.[20] analyzed the effects of equivalence ratio and swirling flow on combustion performance of boron-based solid propellant which contain boron and magnesium particles in the ramjet with a chin-type inlet. B. Kalpakli, et al.[21] developed a detailed computational model for boron particle combustion in varying composition environments for simulations of solid propellant ducted rocket combustion chambers. The model considered the surface and the gas phase reactions with the phase change processes such as melting, solidification, evaporation, and boiling. Z. Xia, et al. [22] researched the details of the combustion processes and flowfields in the secondary combustion chambers and designed two-inlet ducted rocket engine system to improve the combustion efficiency. Y. Kazaoka, et al.[23] measured combustion times of single particles by direct photography and spectroscopic analysis and observed the flame structure of burning particles by schlieren photography, which proved that boron particles burn in two stages separately and the combustion time decrease with increasing temperature. In addition, the ignition and combustion model of boron particles were described in references [24][35].

According to the references above, boron particles burn in two stages separately, i.e. ignition and combustion stages. The ignition process of boron particle results in the removal of the oxide layer covered outside of particle. Then, clean boron reacts with oxygen during the combustion process. In order to be ignited and burned adequately, boron particles need to be blended well with the primary combustion gas and the air entering from intake ports. A swirl flow should improve mixing and residence time leading to improved combustion efficiency[20], [36]-[38]. B. Chen, et al.[20] setup a swirler at the entrance of primary combustion gas and proved that the boron particle

combustion efficiency of the swirl structure was improved by more than 6.5% compared to the non-swirling configuration. However, the swirl number used was not indicated. Swirl generators being installed at the outlets of the engine's bilateral intake ports, H. Wang, Y. Xu, et al.[36] showed that the ignition time and combustion efficiency of boron particles under different swirl numbers in co-swirl and counter-swirl modes. The results showed that the shortest ignition time and the highest combustion efficiency were obtained when the swirl number was 0.385. R. Pern and F. Vinnemeier [37][38] fixed vane swirl generators with a swirl number of 0.54 into the flameholder of solid-fuel ramjet (SFRJ) combustor to determine the influence of swirl flow and fuel composition on boron combustion efficiency. Their results showed that boron combustion efficiency and specific thrust were improved by 10% - 20% for swirl flow conditions. O. Musa, et al.[39][40] studied the effect swirling flow evoked by swirl generator on SFRJ by numerical calculation and experiment. The results showed a positive impact of swirling flow on SFRJ. The regression rate of propellant increased with swirl number increasing. Using swirling flow enhances the flame stability, however, it negatively affected the ignition process and specific impulse. All the swirling flow applications presented above used swirl generators, which would make the ramjet engine complicated. Also, the addition of a swirl generator results in total pressure loss.

On the basis of previous investigations, the work in this paper addresses the gap of powder ramjet and solid ramjet. The concept of HPSR is put forward. And in order to simplify the structure of the engine and reduce total pressure loss, the tangential swirling air intake mode will be used to generate swirling mixing combustion in the second combustion chamber of the HPSR. Also, the effects that different tangential swirl air inlet angles have on the combustion performance of the engine will be studied to provide insight with the aim to understand which configurations have the potential to result in enhanced engine performance.

2. Engine model

Figure 2 illustrates the structure of a HPSR combustion chamber. The total length of the combustion chamber is 700 mm. The diameter is 150mm. Two primary gas nozzles with a diameter of 20 mm, the distance between them is 90mm. The Powder inlet diameter is 12mm. The diameter of the bilateral tangential air intake ports is 40mm. The tangential inlet angle is denoted using α .

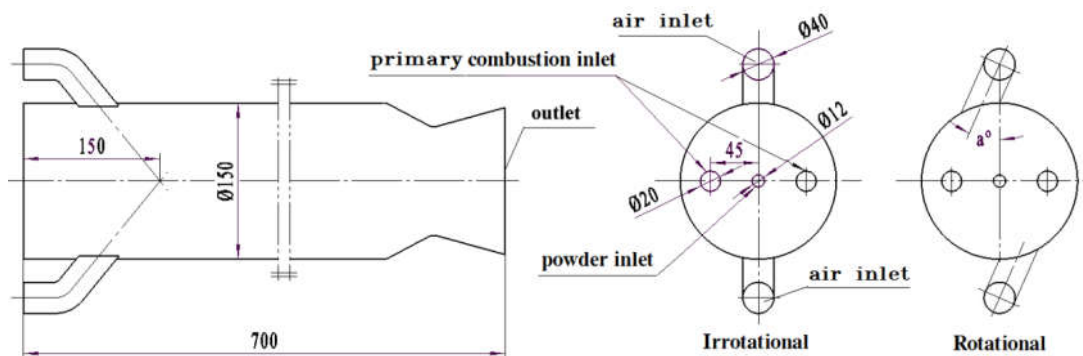


Figure 2 HPSR combustion chamber structure diagram (units are in mm)

In order to simplify the analysis and reduce the difficulty of the numerical calculation, the flow field of the HPSR is

simplified as follows:

- (1). The gas in the secondary combustion chamber is quasi steady flow without heat exchange with its surrounding environment
- (2). Radiation and the body force of the gas are ignored.
- (3). The combustion gas is treated as an ideal gas i.e. abiding by the ideal gas state equation.

3. Numerical Setup

3.1 Governing equation and numerical methods

According to the above assumptions, the governing equations include: the continuum equation, the momentum equation, the energy equation and a transport equation for each component. The form of the general equation in the Cartesian coordinate system can be written as,

$$\frac{\partial(\rho\phi)}{\partial t} + \text{div}(\rho\mathbf{U}\phi) - \text{div}(\Gamma_\phi \text{grad } \phi) = S_\phi \quad (1)$$

where, ϕ is represented as generalized variable, Γ_ϕ is effective transport factor of variable ϕ , S_ϕ is the source term, ρ is the density of fluid, \mathbf{U} is the velocity vector. $\phi, \Gamma_\phi, S_\phi$ have a specific form for a particular equation (shown in Table 1).

Table 1 the form of $\phi, \Gamma_\phi, S_\phi$ in different equation

Equation	ϕ	Γ_ϕ	S_ϕ
Continuum equation	1	0	0
Momentum equation	u_i	μ	$-\frac{\partial p}{\partial x_i} + S_i$
Energy equation	T	$\frac{\lambda}{c_p}$	S_T
Component transport equation	Y_j	D_j	S_j

In the table 1, for the momentum equation, u_i is the fluid velocity, μ is the coefficient of viscosity, p is pressure,

$$S_i = \frac{\partial \tau_{ij}}{\partial x_j}, \quad \tau_{ij} = \mu \left(\frac{\partial u_i}{\partial x_j} + \frac{\partial u_j}{\partial x_i} \right) - \frac{2}{3} \mu \frac{\partial u_k}{\partial x_k} \delta_{ij}, \quad \delta_{ij} = \begin{cases} 1, & j = i \\ 0, & j \neq i \end{cases}, \tau_{ij} \text{ is the viscous stress tensor, } \delta_{ij} \text{ is the}$$

Kronecker delta function. For the energy equation, T is the temperature of fluid, λ is the coefficient of thermal conduction, c_p is the specific thermal capacity, S_T is the source term of temperature which resulted by the heat of reaction and phase transformation latent heat. For the component transport equation, Y_j is the mass fraction of species j , D_j is diffusion coefficient of species j in the flow, S_j is the source of species j which resulted by reaction.

The trajectories of particles are traced by the Lagrangian particle trajectory model[41]. The effect of particles on gas phase is considered by adding source term to the gas phase governing equation. Realizable k-ε model[42] with swirl modification was used to address turbulence. It not only preserves the advantages of the convergence stability and appropriate accuracy of the standard k-ε model, but also modifies the model used for complex flow field with large pressure gradient or vortex.

3.2 Combustion model

3.2.1 Gas phase combustion model

The species of HTPB pyrolysis products include CO, H₂, CO₂, H₂O, N₂ mainly and a small amount of HCl, Cl, H, NH₃, HO[43]. To facilitate calculation, it is assumed that the combustion ingredients of fuel-rich HTPB propellant in the combustion gas generator consists of CO, H₂, CO₂, H₂O and N₂. Among them, CO and H₂ will react with oxygen in the air coming from the inlet, and the chemical equation of the combustion reactions as follows,



The gas phase combustion model employs the Eddy-Dissipation Model (EDM)[44], which can effectively control the net reaction rate of each component and calculate the chemical reaction process of the complex flow inside the afterburner chamber of solid ramjet or HPSR.

3.2.2 boron particle ignition and combustion model

Boron particles burn in two stages separately, i.e. ignition and combustion stages. The boron particle ignition model is based on the multi-layer oxide structure proposed in literature[32][33]. Figure 3 shows the reaction mechanism of boron particle ignition process. To some extent, the ignition process of boron particle means the removal of the inhibiting oxide layer. As is shown in figure 3, the layer of (BO)_n(l) is generated by the dissolution reaction between boron and B₂O₃(l). Then, (BO)_n(l) diffuses outward and reacts with oxygen. A liquid layer of B₂O₃(l) (outermost layer) is generated on the surface of the oxide layer. The evaporation rate of B₂O₃(l) is pressure-dependent. With the increasing of temperature, the evaporation rate can be higher, and the phenomenon of the outermost layer consumption happens. Therefore, the outermost layer will be consumed completely before the end of the ignition process. Finally, the oxide layer presents a two-layer structure (see the right half of the Figure 3). Both the evaporation and heterogeneous reaction with oxidants on the surface will change. There is a tiny flame on the surface of the oxide layer during the first-stage combustion. The boundary between the ignition delay and the first-stage combustion can be told apart by the structure change of the oxide layer (whether x_o=0). The particle temperature at that moment is defined as the ignition temperature.

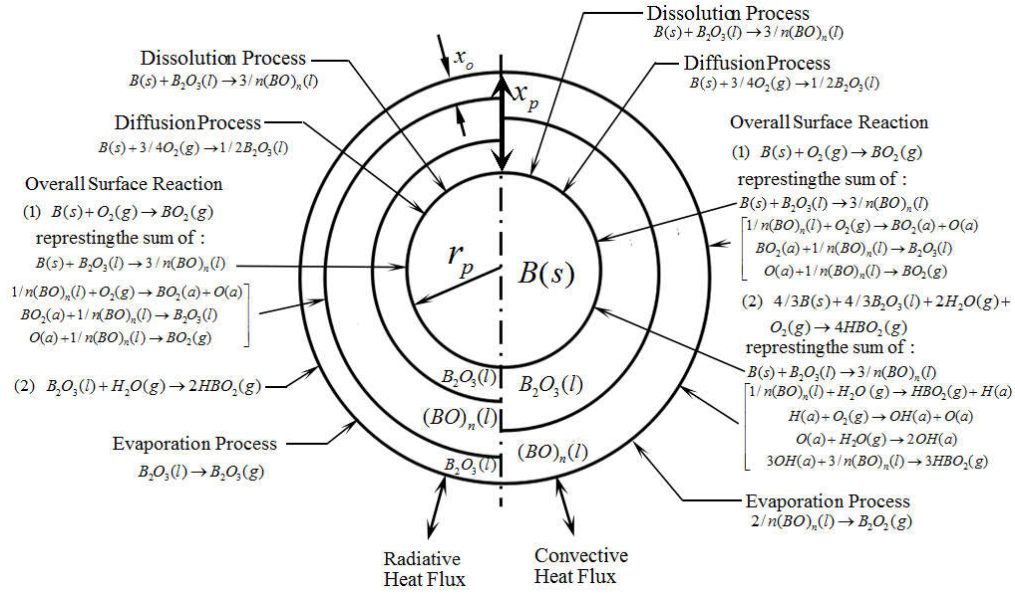


Figure 3 Reaction mechanism of boron particle ignition process

The governing equations for the consumption of the particles and the removal of oxide layer can be written as:

$$\frac{dr_p}{dt} = \begin{cases} \left[-\left(1 - \frac{1}{2}\theta\right)R_{BO_2} - \frac{1}{2}\theta R_B \right] \frac{M_B}{\rho_B} & (x_o > 0) \\ \left[-\frac{2}{3}R_{EB_2O_2} - \frac{2}{3}R_{H_2O} - \left(1 - \frac{1}{2}\theta\right)R_{BO_2} - \frac{1}{2}\theta R_B \right] \frac{M_B}{\rho_B} & (x_o \leq 0) \end{cases} \quad (4)$$

$$\frac{dx}{dt} = \begin{cases} \left(\frac{1}{4}\theta R_B - R_{EB_2O_3} - R_{H_2O} \right) \frac{M_{B_2O_3}}{\rho_{B_2O_3}} & (x_o > 0) \\ \left(\frac{1}{4}\theta R_B - \frac{2}{3}R_{EB_2O_2} - \frac{2}{3}R_{H_2O} \right) \frac{M_{B_2O_3}}{\rho_{B_2O_3}} & (x_o \leq 0) \end{cases} \quad (5)$$

$$\frac{dx_o}{dt} = \begin{cases} \left[\left(1 - \frac{1}{2}\theta R_{BO_2}\right) - R_{EB_2O_3} \right] \frac{M_{B_2O_3}}{\rho_{B_2O_3}} & (x_o > 0) \\ \left[\left(1 - \frac{1}{2}\theta R_{BO_2}\right) - R_{EB_2O_3} - R_{H_2O} \right] \frac{M_{B_2O_3}}{\rho_{B_2O_3}} & (x_o \leq 0) \end{cases} \quad (6)$$

$$\frac{dT_p}{dt} = \begin{cases} \frac{4\pi(r_p + x)^2 \left[-\left(1 - \frac{1}{2}\theta\right)R_{BO_2}Q_2 - R_{EB_2O_3}Q_5 - \frac{1}{2}\theta R_B Q_4 - R_{H_2O}Q_6 + h_c(T_\infty - T_p) + \sigma\epsilon_B(T_\infty^4 - T_p^4) \right]}{\frac{4}{3}\pi r_p^3 \rho_B C_{p_B} + 4\pi r_p^2 x \rho_{B_2O_3} C_{p_{B_2O_3}}} & (x_o > 0) \\ \frac{4\pi(r_p + x)^2 \left[-R_{EB_2O_2}Q_1 - \left(1 - \frac{1}{2}\theta\right)R_{BO_2}(Q_2 + Q_5) - R_{H_2O}Q_3 - \frac{1}{2}\theta R_B Q_4 + h_c(T_\infty - T_p) + \sigma\epsilon_B(T_\infty^4 - T_p^4) \right]}{\frac{4}{3}\pi r_p^3 \rho_B C_{p_B} + 4\pi r_p^2 x \rho_{B_2O_3} C_{p_{B_2O_3}}} & (x_o \leq 0) \end{cases} \quad (7)$$

Where, x_o is the thickness of outer oxide layer, x is the thickness of the overall oxide layer, θ is oxygen diffusivity to particle surface and the value of θ is detailed in references [34,35]. R_i is the molar reaction rate of the global reaction, M_i is the molecular weight, ρ_i is the density, Q_j is the heat of every global reaction, r_p is the

radius of the particle, T_p is the temperature of particle, T_∞ is the ambient temperature, C_p is the specific heat, σ is the Boltzmann constant, h_c is the convective heat transfer coefficient, ε_b is the emissivity of the boron particle. Calculations or values of these parameters are found in the literature[32][33].

After ignition is completed, boron particles enter the burning stage. Regardless of combustion multi-step reaction, the total combustion equation for boron particle can be written as:



the boron particle burning rate[25] is listed below as:

$$\dot{m} = 4\pi r_p \rho D \ln(1 + 0.676Y_{O_2,\infty}) \quad (9)$$

where, r_p is represents the particle radius, ρD is the product of the gas density and the diffusion coefficient of the ambient particles (a value of $2 \times 10^{-4} \text{ kg/m}^2 \cdot \text{s}$ was used in this work), $Y_{O_2,\infty}$ is the mass fraction of oxygen in the ambient gas of the particles.

3.3 Mesh and Boundary Conditions

The computational domain and grid were generated using the commercial software ICEM[45]. A multiblock grid approach was used (as shown in Figure 4). Cells are highly concentrated close to the wall surface, the primary combustion inlet and the powder inlet to ensure the accuracy of the numerical simulation. The height of the first row of cells is set a distance of 0.1 mm for the walls, and the total number of cells is 870535.

The simulated flight conditions correspond to an altitude of 20,000m and the Mach number is 3. The boundary conditions are shown in Table 2. The mass fraction of primary combustion gas CO、H₂、CO₂、H₂O and N₂ is 45%, 20%, 10%, 5% and 20% respectively. The mass flow rate is 0.26kg/s, the total temperature is 1800K. Boron powder is fluidized by gas N₂ its mass flow rate is 0.02kg/s, the total temperature is 300K; air mass flow rate is 4kg/s, the total temperature is 573K, outlet pressure is 0.06MPa, temperature is 255K; boron particles mass flow rate is 0.1 kg/s. The primary diameter of boron particles is 5μm, the thickness of the oxide layer is 1.3% of the particle radius, the initial temperature is 300K, the wall-normal reflect coefficient is 0.7 and the tangential reflect coefficient is 0.72.

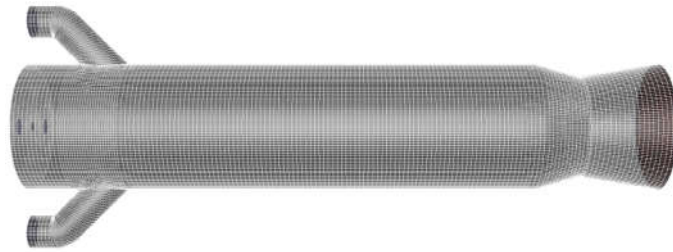


Figure 4 Mesh applied in computational fluid dynamics

Table 2 boundary conditions

Boundary name	Boundary type	Mass flow rate	Gauge pressure	Total temperature	Species	Discrete phase
---------------	---------------	----------------	----------------	-------------------	---------	----------------

		(kg/s)	(MPa)	(K)		
air inlet	mass flow rate	4	0.5	573	22% O ₂ , 78% N ₂	reflect
Primary combustion inlet	mass flow rate	0.26	0.4	1800	45% CO, 20% H ₂ , 10% CO ₂ , 50% H ₂ O, 20% N ₂	reflect
powder inlet	mass flow rate	0.02	0.1	300	N ₂	reflect
outlet	pressure outlet	---	0.06	255	---	escape
wall	no slip wall	---	---	---	---	reflect
Boron particles	Surface injection	0.1	---	300	B	---

4. Results and discussion

4.1 Test cases

In order to analyze the effect of the tangential air inlet angle on the ignition distance boron particles and combustion efficiency of HPSR, six angles were chosen from 0° to 25°. The cases are shown in the table 3.

Condition	Different tangential air inlet angle α (°)
Case A	0
Case B	5
Case C	10
Case D	15
Case E	20
Case F	25

4.2 Particle trajectory and ignition distance of boron particles

Ignition distance is the distance between the inlet port of boron particles and the position where the oxide layer is depleted. Figure 5 shows that the oxide layer of boron particles changes with particle trajectory. It can be seen that the particles with fluidizing gas enter the combustion chamber from the central inlet. At first, particles are located near the center line of chamber. When the tangential angle of the air intake is 0° (see Case A), boron particles are impinged by air jets and move toward the wall. Due to the wall-attachment effect[46] of the air flow and the influence of local airflow pulsation, boron particles move in the recirculating zone with the air flow toward the head of combustion chamber, and then move toward the nozzle exit along with the air flow. When the tangential angle of air intake is 5°, 10°, 15°, 20° and 25° (see Case B-F), the particles exhibit a swirling mixing motion after the air inlet ports, and the number of particles entering the head decreases with the increase of the tangential swirl angle. This is mainly because the larger the tangential swirl angle, the smaller the interaction of the air flow, the smaller the velocity of the recirculating air flow, and the air flow can carry fewer particles back to the head. But the particles trajectory are more disordered with the increase of tangential angle of air intake after the air inlet.

According to Fig.5, the thickness change of boron particles oxide layer have the same trend for all cases. Ignition is completed near the air inlet port. However, the ignition distance of the case B and C is less than that of case A, E, D and F. The ignition distance of case A, B, C, D, E and F are the 185mm, 132mm, 131mm, 163mm, 188mm and

195mm respectively.

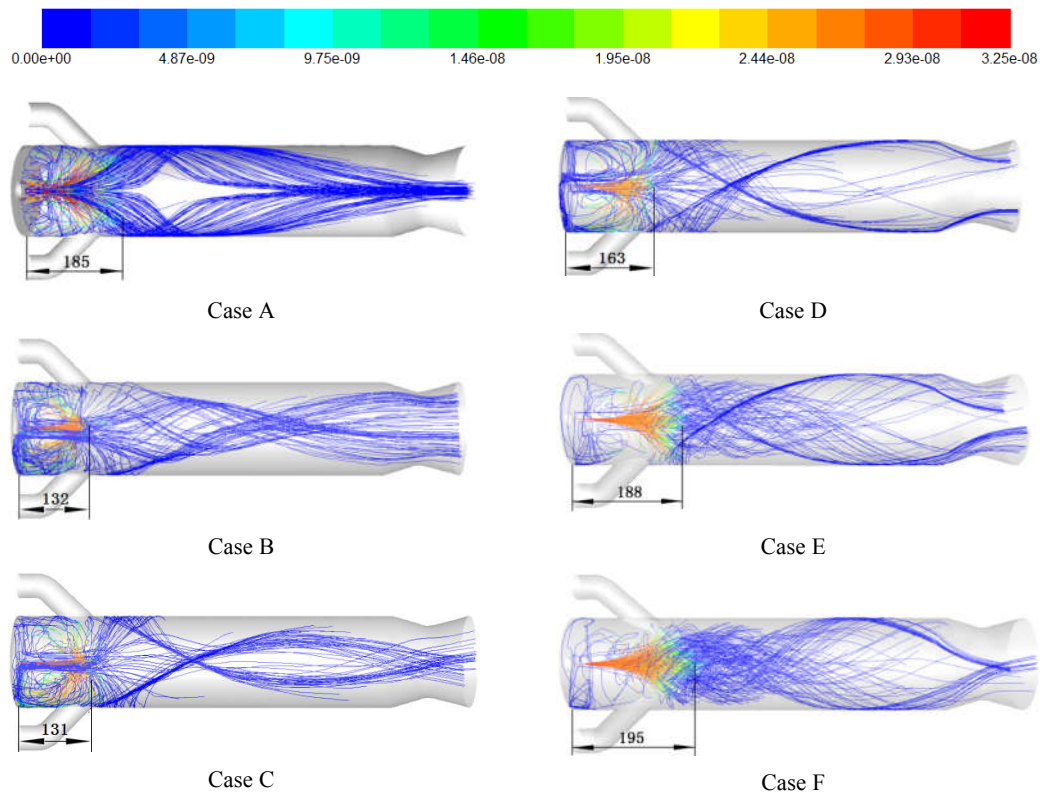


Figure 5 oxide layer of boron particles change with particle trajectory

In order to further illustrate the trend of particle trajectory as shown in Fig.5, the vorticity distribution within the combustion chamber is analyzed by taking a cross section every 150mm along the axial direction of the combustion chamber under various cases (see Fig.6). It can be seen from the diagram that 1) the vorticity in the combustor head is the largest, because the jet impinges and ejects in the confined space to form vortices, but the vorticity decreases rapidly from the downstream of the air inlet to the combustor outlet; 2) With the increase of tangential air inlet angle, the vorticity in the combustor head increases from 0° to 10° , but decreases gradually from 10° to 25° , while the vorticity increases from the downstream of the air inlet to the combustor outlet. In order to understand the change of vorticity in more detail, Figure 7 shows the mean vorticity of the cross-section of combustion chamber at all cases. It can be seen that the vorticity of tangential air inlet angle at 10° is the largest at $x < 450\text{mm}$, the next is at the 5° . This is why the ignition distance of the case B and C are less than that of case A, E, D and F.

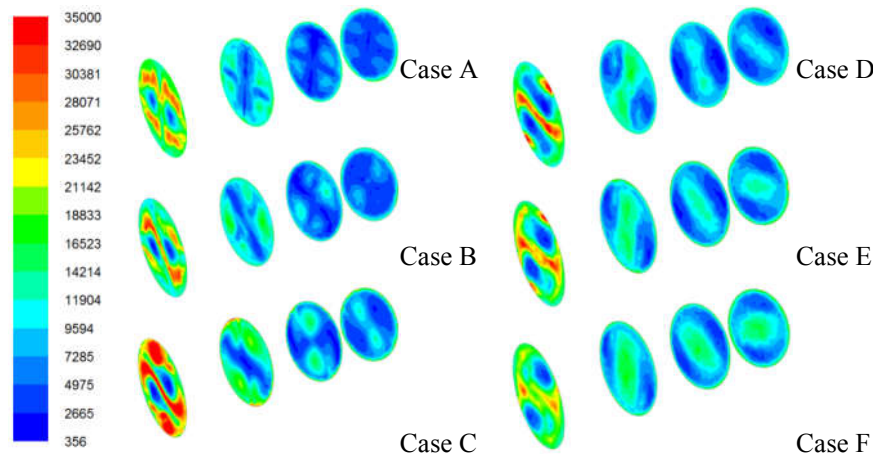


Figure 6 Vorticity distribution in the cross-section of combustion chamber at all cases

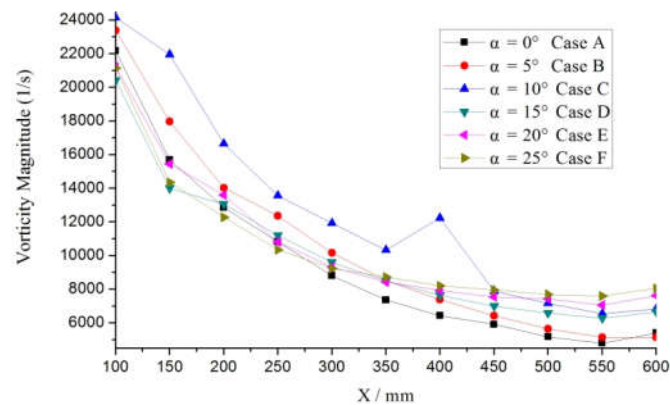


Figure 7 Mean vorticity of the cross-section of combustion chamber at all cases

4.3 Temperature distribution

In order to intuitively judge the effect of different tangential swirl inlet angles on combustion performance of boron HPSR, the temperature distributions of various sections and walls of the combustion chamber are shown in Figure 8. And for quantitative analysis of temperature distribution, Figure 9 shows the mean temperature of section of the combustion chamber for all the test cases considered in this work. It shows that the temperature from the combustion chamber head to the air inlet is lower. For example, the mean temperature is in the range of 1600K-1800K except that 2200K of case C when the section is at $x=100$. When the tangential angle of air inlet is 0° , the low temperature region near the air inlet is the largest and the temperature in the whole combustion chamber is lower because of the large impulse and the deep penetration of the air jet. According to the air concentration zone shown in the Fig.8, it will be divided into two parts when tangential swirl air intake angle is 10° and it is greater the distance with the increase of angle, which results in combustion zone being divided into two parts. It is seen obviously that the temperature in the combustion chamber downstream of the intake port differentiates with the tangential angle of air inlet. The temperature at the center of the combustion chamber for case C (i.e. 10° tangential swirl angle of air intake) is the highest and is well-distributed. With further increasing the tangential

angle, a high temperature zone shifts closer to the wall. A two-zone distribution of high and low temperature is formed on the wall. This will translate into practical challenges for accomplishing thermal shielding.

According to Figure 9, it can be seen that the temperature of case C is much more than that of other cases at the cross sections for $x < 350$ mm. Also, the uniformity of the temperature distribution is better than that of any other cases because the mean temperature of section changes in the small range of 2177K to 2560K for the case C.

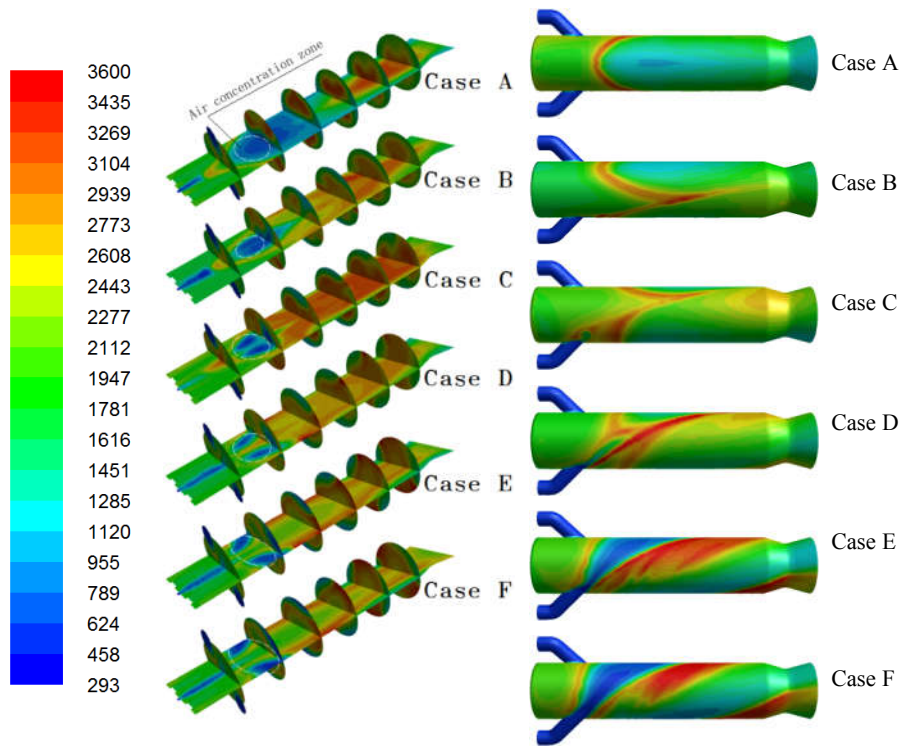


Figure 8 Section and wall temperature distribution of the combustion chamber in all cases

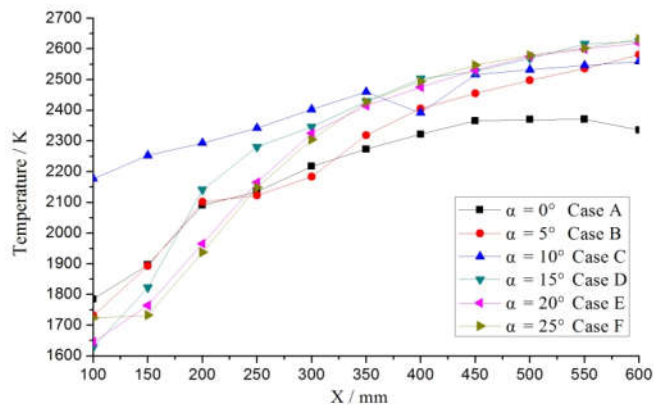


Figure 9 Mean temperature of section of the combustion chamber in all cases

4.4 Combustion efficiency

4.4.1 Method for Calculating the Combustion Efficiency

Component combustion completion rate[36] is used to express the combustion efficiency of HPSR. Secondary

combustion efficiency of gas phase components at any cross section is defined as follows:

$$\eta_{i,g} = \left(1 - \frac{\int_A \rho u Y_{i,g} dA}{\dot{m}_{i,g}}\right) \quad (6)$$

where, $\eta_{i,g}$, $Y_{i,g}$, $\dot{m}_{i,g}$ are the combustion efficiency, mass fraction and total flow rate of the combustible gas in the section i respectively. ρ and u are the density and velocity of fluid at the section i . Then, the total combustion efficiency of gas is as follows:

$$\eta_g = \frac{Q_{CO}\lambda\eta_{CO} + Q_{H_2}(1-\lambda)\eta_{H_2}}{Q_{CO}\lambda + Q_{H_2}(1-\lambda)} \quad (7)$$

where, η_{CO} , η_{H_2} are the combustion efficiency of CO , H_2 respectively; λ is the fraction of CO in the combustible gas; Q_{CO} and Q_{H_2} are combustion heat of CO , H_2 respectively.

The combustion efficiency of boron particles at any cross section is defined as follows:

$$\eta_B = 1 - \frac{\int_A \dot{m}_B dA}{\dot{m}_{B0}} \quad (8)$$

where, \dot{m}_{B0} is the mass rate of boron particles at the entrance, \dot{m}_B is the residual mass flow rate of boron particles on this section. The total combustion efficiency at any cross section can be expressed as:

$$\eta = \frac{\sum_{i=1}^{N_c} (Y_{i,g} / \sum_{j=1}^{N_c} Y_{j,g}) \eta_{i,g} Q_{i,g} + \eta_B \cdot \dot{m}_{B0} \cdot Q_B}{\sum_{i=1}^{N_c} (Y_{i,g} / \sum_{j=1}^{N_c} Y_{j,g}) Q_{i,g} + \dot{m}_{B0} \cdot Q_B} \quad (9)$$

where, N_c is the number sort of combustible gas, $Q_{i,g}$, Q_B are the heat of combustion of gas and boron particles respectively. The value of Q_{H_2} , Q_{CO} and Q_B are $1.208 \times 10^8 J/kg$, $1.01 \times 10^7 J/kg$ and $1.17 \times 10^8 J/kg$ according to reference[25] respectively.

Figure 10 shows the change of combustion efficiency of CO and H_2 along the axial section in combustion chamber under different cases. The combustion efficiency of the gas at the combustion chamber cross section increases rapidly with the increase of the axial distance. For CO , when the axial position reaches 400 mm, the combustion efficiency of the case A to case D reaches more than 90%, and the combustion efficiency at the outlet of the combustion chamber reaches 100% almost; The combustion efficiency of case E to case F is low relatively, and it is 94.8% and 94.2% at the exit of combustion chamber respectively. For H_2 , the combustion efficiency increases slowly relative to that of CO along the axial position. The combustion efficiency at the exit of combustion chamber from Case A to Case F are 99.94%, 98.15%, 99.29%, 98.08%, 80.54% and 80.88% respectively. According to the analysis, the tangential swirl air inlet angle has a certain influence on the gas phase combustion efficiency. When

the tangential swirl air inlet angle is greater than 15 degrees, the combustion efficiency decreases significantly.

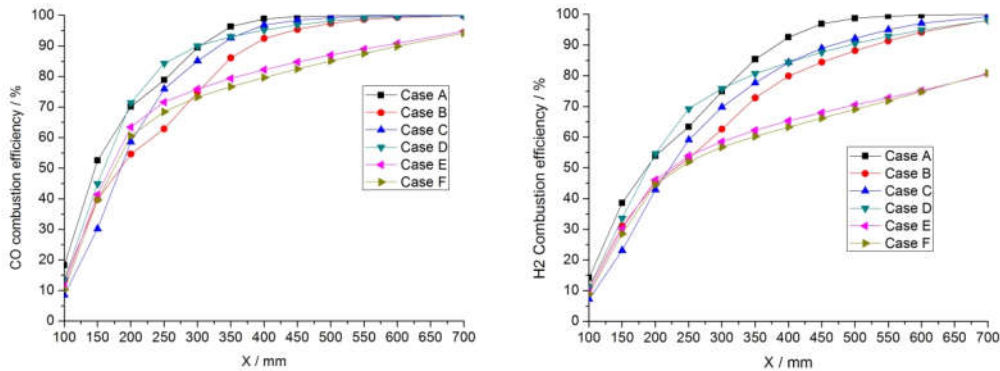


Figure 10 The variation law of CO and H2 combustion efficiency along the axial section

Figure 11 shows the variation of the combustion efficiency of boron particles along the axial section in the combustion chamber for the different cases examined. Undoubtedly, with the increase of the axial distance, the boron particles combustion efficiency at the cross section of the combustor increases, but the increase speed slows down compared with that of the gas combustion efficiency. In case A, when the tangential swirl air inlet angle is 0 degrees, the combustion efficiency increases rapidly in the first half of the combustor, but slowly in the second half, and the combustion efficiency at the exit is 88.34%. The combustion efficiency of case E and case F in the first half of the combustor is low, and the combustion efficiency at the exit is 89.80% and 82.51%, respectively. Comparing the combustion efficiency of all cases at the exit, it can be seen that the combustion efficiency increases from case A to case C and decreases from case C to case F. That is, the combustion efficiency of particles in case C is maximum, and it is 94.76%.

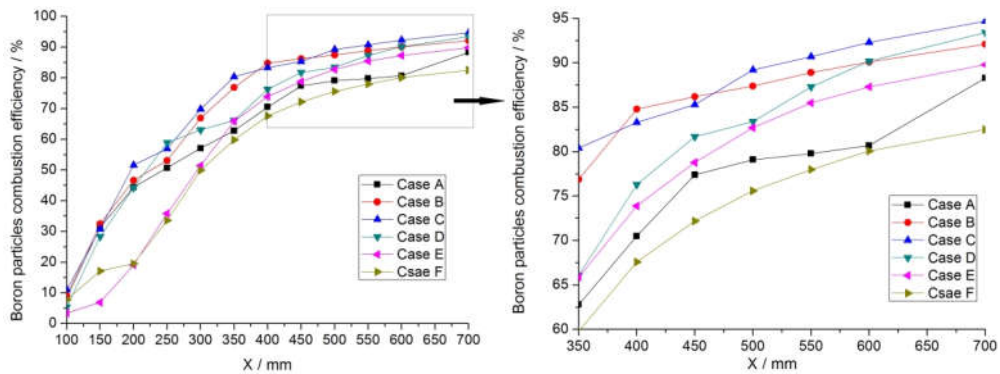


Figure 11 the variation of the combustion efficiency of boron particles along the axial section

Table 4 shows the statistical result of the combustion efficiency in different cases. This table shows that with the increase of the tangential angle of the inlet, the total combustion efficiency increases at first and then decreases later and the maximum combustion efficiency lies in case C, i.e. when the tangential swirl angle of air is 10 degrees, the combustion efficiency is the highest.

Table 4 the combustion efficiency under different cases

Case	CO(%)	H2(%)	Boron Particle (%)	total (%)
------	-------	-------	--------------------	-----------

A (0°)	99.99	99.94	88.34	92.84
B (5°)	99.84	98.15	92.13	94.57
C (10°)	99.98	99.29	94.76	96.52
D (15°)	99.88	98.08	93.35	95.29
E (20°)	94.80	80.55	89.80	87.06
F (25°)	94.21	80.88	82.51	82.67

5. Conclusion

A hybrid powder-solid ramjet (HPSR) configuration was investigated. Boron particles were used as the powder propellant. Thrust regulation when using a solid-only ramjet is highly limited. However, hybridization using a powder propellant provides a means to regulate the thrust generated by the engine. A numerical investigation of the fluid flow and combustion in a boron HPSR was carried out. The focus of this work was to gain a better understanding of the effects that the tangential air inlet angle has on the ignition response of the boron particles, as well as the combustion efficiency of the HPSR configuration tested. As a result of the simulations performed, the following conclusions can be drawn:

- (1) The ignition distance of boron particles decreases with the tangential swirl air inlet angle increasing from 0° to 10°, while it increases with tangential swirl air inlet angle increasing from 10° to 25°. The minimal ignition distance of particles occurs when the tangential swirl air inlet angle is 10° for the conditions tested in this work.
- (2) The temperature of the cross sections $x < 350$ mm for the case of 10° tangential swirl angle is much more than that of other cases. The uniformity of the temperature distribution is better than that of any other working conditions.
- (3) The tangential swirl air inlet angle has a certain influence on the gas phase combustion efficiency. When the tangential swirl air inlet angle is greater than 15°, the combustion efficiency decreases significantly.
- (4) The combustion efficiency of boron particles increases with the tangential swirl air inlet angle when it changes from 0° to 10°, while it decreases with tangential swirl air inlet angle when it is increased from 10° to 25°. The maximum combustion efficiency of particles and the total combustion efficiency of the boron HPSR occur when the tangential swirl air inlet angle is 10° for the conditions tested in this work.

References

- [1] B. Natan and A. Gany, Ignition and Combustion of Boron Particles in the Flowfield of a Solid Fuel Ramjet, *J. Propulsion*. 7 (1991) 37-43.
- [2] A. Gany, Thermodynamic limitation on boron energy realization in ramjet propulsion, *Acta Astronautica*. 98 (2014) 128–132.
- [3] J. Sender and H. K. Ciezki, Velocities of Reacting Boron Particles within a Solid Fuel Ramjet Combustion Chamber, *Defense Science Journal*. 48 (1998) 343-349.
- [4] E. T. Sandall, J. Kalman, J. N. Quigley, S. Munro, T. D. Hedman, A study of solid ramjet fuel containing boron–magnesium mixtures, *Propulsion and Power Research*. 6 (2017) 243-252.
- [5] W. Jung and S. Baek et al, Combustion Characteristics of Ramjet Fuel Grains with Boron and Aluminum Additives, *Journal of Propulsion and Power*. 34 (2018) 1070-1079.
- [6] V. Rodić, M. Petrić, The Effect of Additives on Solid Rocket Propellant Characteristics, *Scientific Technical Review*. 54 (2004) 9-13.
- [7] S. A. Rashkovskiy, Formation of solid residues in combustion of boron containing solid propellants, 7th European Conference for Aeronautics and Space Sciences (EUCASS), DOI: 10.13009/EUCASS2017-105.

- [8] T. L. Varghese, R. Muthiah, J. David, A. J. Kurian, S. K. Athithan, V. N. Krishnamurthy and M. R. Kurup, Studies on Composite Extrudable Propellant with varied Burning Rate Pressure Index 'n', *Defence Science Journal*. 39 (1989) 1-12.
- [9] NASA, Solid rocket thrust vector control, NASA-SP-8114, 1974.
- [10] J. Chang, B. Li, W. Bao, W. Niu, D. Yu, Thrust control system design of ducted rockets, *Acta Astronautica*. 69 (2011) 86-95.
- [11] H. J. Loftus, L. N. Montanino, R. C. Bryndle, Powder rocket feasibility evaluation, *AIAA* 72-1162, 1972.
- [12] M. Shorr, T. F. Reinhardt, Feasibility of a fluidized powder demand-mode gas generator, *J. Spacecr. Rockets*. 11 (1974) 29–32.
- [13] S. Goroshin, A. Higgins, M. Kamel, Powdered metals as fuel for hypersonic ramjets, *AIAA-2001-3919*, 2001.
- [14] Z. Xia, H. Shen, J. Hu, B. Liu, Experimental Investigation of Powdered Metals Fuel Ramjet, *AIAA* 2008-5131, 2008.
- [15] C. Li, C. Hu, X. Xin, Y. Li, H. Sun, Experimental study on the operation characteristics of aluminum powder fueled ramjet, *Acta Astronautica*. 129 (2016) 74–81.
- [16] T. V. Chelaru, F. Mingireanu, Hybrid rocket engine, theoretical model and experiment, *Acta Astronautica*. 68 (2011) 1891–1902.
- [17] V. B. Betelin, A.G. Kushnirenko, N. N. Smirnov, V. F. Nikitin, V. V. Tyurenkova, L. I. Stamov, Numerical investigations of hybrid rocket engines. *Acta Astronautica*, 144 (2018) 363–370.
- [18] T. dawara, M. Tanabe, T. Kuwahara, Ignition Characteristics of Boron Particles in Ducted Rockets, *AIAA-2005-4498*, 2005.
- [19] A. Gany, Comprehensive Consideration of Boron Combustion in Air- breathing Propulsion, *AIAA* 2006-4567, 2006.
- [20] B. Chen, Z. Xia, L. Huang, L. Ma, Characteristics of the combustion chamber of a boron-based solid propellant ducted rocket with a chin-type inlet. *Aerospace Science and Technology*. 81-82 (2018) 210-219.
- [21] B. Kalpakli, E. B. Acar, A. Ulas, Improved combustion model of boron particles for ducted rocket combustion chambers, *Combustion and Flame*. 179 (2017) 267–279.
- [22] Z. Xia, J. Hu, D. Fang, J. Guo, W. Zhang, Combustion Study of the Boron Particle in the Secondary Chamber of Ducted Rocket, *AIAA* 2006-4445, 2006.
- [23] Y. Kazaoka, K. Takahashi, M. Tanabe, T. Kuwahara, Combustion Characteristics of Boron Particles in The Secondary Combustor of Ducted Rockets, *AIAA* 2011-5867, 2011.
- [24] M. K. King, Ignition and Combustion of Boron Particles and Clouds, *J. Spacecraft*. 19 (1982) 294-306.
- [25] S. C. Li, F. A. Williams, Ignition and combustion of boron in wet and dry atmospheres, *Symposium (International) on Combustion*. 23 (1990) 1147-1154.
- [26] C. L. Yeh, K. K. Kuo, Ignition and combustion of boron particles. *Progress in Energy and Combustion Science*. 22 (1996) 511-541.
- [27] B. Hussmann, M. Pfitzner, Extended combustion model for single boron particles – Part I: Theory, *Combustion and Flame*. 157 (2010) 803–821.
- [28] B. Hussmann, M. Pfitzner, Extended combustion model for single boron particles –Part II: Validat, *Combustion and Flame* 157 (2010) 822–833.
- [29] D. Liang, J. Liu, J. Xiao, J. Xi, Y. Wang, Y. Zhang, J. Zhou, Energy release properties of amorphous boron and boron-based propellant primary combustion products, *Acta Astronautica*. 112 (2015) 182–191.
- [30] D. Meinköhn, The Effect of Particle Size and Ambient Oxidizer Concentration on Metal Particle Ignition, *Combustion Science and Technology*. 181 (2009) 1007-1037.
- [31] W. Ao, Y. Wang, S. Wu, Ignition kinetics of boron in primary combustion products of propellant based on its unique characteristics, *Acta Astronautica*. 136 (2017) 450–458.
- [32] X. Hu, Y. Xu, W. Ao, Z. Zeng, C. Hu, X. Zhu, Ignition model of boron particle based on the change of oxide layer structure, *Proceedings of the Combustion Institute*. 37 (2019) 3033-3044.
- [33] Y. Xu, X. Hu, H. Zou, Y. Li, Z. Zeng, Research on Model of Ignition of Boron Particle Based on Multiple Oxide Layer Structure, *Acta Armamentarii*. 37 (2016) 2242-2250.
- [34] A. Povitsky, Y. Goldman. Boron particle ignition in high-speed flow. *AIAA* 93-2202, 1993.
- [35] I. Glassman, F. A. Williams, P. Antaki, A physical and chemical interpretation of boron particle combustion. *Symposium (International) on Combustion*. 20 (1985) 2057-2064.
- [36] H. Wang, Y. Xu, X. Hu, Z. Zeng. Research on the Characteristics of Secondary Combustion of Boron-Based Ducted Rockets with Swirling Air Injection. *Acta Armamentarii*. 36 (2015) 619-625.
- [37] R. Pern and F. Vinnemeier, The Influence of Swirl and Fuel Composition of Boron-Containing Fuels on Combustion in a Solid Fuel Ramjet Combustion Chamber. *AIAA* 89-2885, 1989.
- [38] R. Pern and F. Vinnemeier, Swirl and Fuel Composition Effects on Boron Combustion in Solid-Fuel Ramjets, *Journal of Propulsion and Power*. 8 (1992) 609-614.
- [39] O. Musa, X. Chen, C. Zhou, Combustion characteristics and turbulence modeling of swirling reacting flow in solid fuel ramjet, *Acta Astronautica*. 139 (2017) 1–17.
- [40] O. Musa, X. Chen, C. Zhou, Experimental investigation on the effect of swirling flow on combustion characteristics and performance of solid fuel ramjet, *Acta Astronautica*. 148 (2018) 163–174.
- [41] S. A. Morsi and A. J. Alexander, An Investigation of Particle Trajectories in Two-Phase Flow Systems. *Journal of Fluid Mechanics*. 55 (1972) 193-208.
- [42] T. H. Shih, W. W. Liou, A. Shabbir, Z. Yang, and J. Zhu, A New k-ε Eddy-Viscosity Model for High Reynolds Number Turbulent Flows - Model Development and Validation, *Computers Fluids*. 24 (1995) 227–238.
- [43] W. Cai, P. Thakre, V. Yang, A model of AP/HTPB composite propellant combustion in rocket-motor environments, *Combustion Science and Technology*. 180 (2008) 2143–2169.
- [44] B. F. Magnussen and B. H. Hjertager. On mathematical models of turbulent combustion with special emphasis on soot

formation and combustion. Symposium (International) on Combustion. 16 (1977) 719-729.

[45] ANSYS Inc., Ansys ICEM CFD User's Manual. Canonsburg, PA 15317, 2013.

[46] W. Nie, Y. Liu, W. Wei, X. Hu, X. Ma, H. Peng, Effect of suppressing dust by multi-direction whirling air curtain on fully mechanized mining face, International Journal of Mining Science and Technology, 26 (2016) 629–635.

Acknowledgments

This work was supported by National Natural Science Foundation of China (No. 51666012)

Data article

Title: Data of ignition and combustion of a hybrid powder-solid ramjet under different tangential swirl air inlet angle

Authors: Yihua Xu^(a), Rui Jia^(a), Humberto Medina^(b), Haijun Sun^(a)

Affiliations: (a) School of Aircraft Engineering, Nanchang Hangkong University, Nanchang, Jiangxi, 330063, PR China

(b) School of Mechanical, Aerospace and Automotive Engineering, Coventry University, Coventry, CV1 5FB, UK

Contact email: xuyihua2003@163.com

Abstract: This article contains data on ignition and combustion of a hybrid powder-solid ramjet under different tangential swirl air inlet angle. A new ramjet configuration using powder and solid fuel as propellant is put forward, namely, hybrid powder-solid ramjet (HPSR). Boron particles were used as the powder. The data of ignition distance of boron particles, the distribution of vorticity, temperature in the HPSR and the combustion efficiency of a HPSR with different tangential air inlet angles (0° , 5° , 10° , 15° , 20° , 25°) are shown here through cloud pictures, charts and tables. These data can be also found in the paper "Effect of tangential swirl air inlet angle on the combustion efficiency of a hybrid powder-solid ramjet".

Specifications Table

Subject area	<i>Physics, Chemistry</i>
More specific subject area	<i>Space propulsion, ramjet</i>
Type of data	<i>Table, figure</i>
How data was acquired	<i>Numerical calculation</i>
Data format	<i>Raw, filtered, analyzed</i>
Experimental factors	<i>Establishment of ignition and combustion model of boron particles, selection of appropriate turbulence model, particle trajectory model.</i>
Experimental features	NA
Data source location	<i>School of Mechanical, Aerospace and Automotive Engineering, Coventry University, UK</i>
Data accessibility	<i>Data is available with the article</i>

Value of the data

- The data is used for researching new ramjet configuration using powder and solid fuel as propellant (HPSR).
- The data present the construction of HPSR.
- The presented data provide details on ignition of boron in the HPSR.

- This data shows evidence of the effects of tangential air inlet angles on the combustion efficiency of HPSR.

1. Data

The data in this paper are calculated for the combustion flow of hybrid powder-solid ramjet (HPSR). The aim is to verify the effect of swirl inlet angle on ignition combustion of particles and total combustion efficiency in the HPSR. The data include ignition distance of boron particles (see Fig. 3), the vorticity distribution (see Fig. 4), the mean vorticity of the cross-section of combustion chamber (see Fig. 5), the temperature distributions (see Fig. 6), the mean temperature of section of the combustion chamber(see Fig. 7), the change of combustion efficiency of CO and H₂(see Fig.8), combustion efficiency of boron particles(see Fig. 9) and the combustion efficiency in different cases(see Table 3).

2. Experimental Design and Methods

2.1 Design

Figure 1 shows the construction of a HPSR. The main components include a combustion gas generator, a powder injector, an air inlet, a second combustion chamber and a nozzle. The operation principle of HPSR is that the solid powder is sprayed from the head of the second combustion chamber, the air from the intake port provides sufficient oxygen, and the high temperature gas from the gas generator provides sufficient high temperature environment to ensure that the solid particles are fully burned in the afterburner to increase the working temperature and total pressure, which results in improving of engine performance.

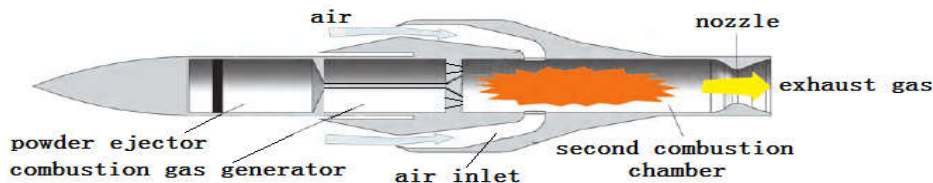


Figure 1 Hybrid powder-solid ramjet sketch

Figure 2 illustrates the structure of a HPSR combustion chamber. The total length of the combustion chamber is 700 mm. The diameter is 150mm. Two primary gas nozzles with a diameter of 20 mm, the distance between them is 90mm. The Powder inlet diameter is 12mm. The diameter of the bilateral tangential air intake ports is 40mm. The tangential inlet angle is denoted using α . Six angles were chosen from 0° to 25° (shown in the table 1).

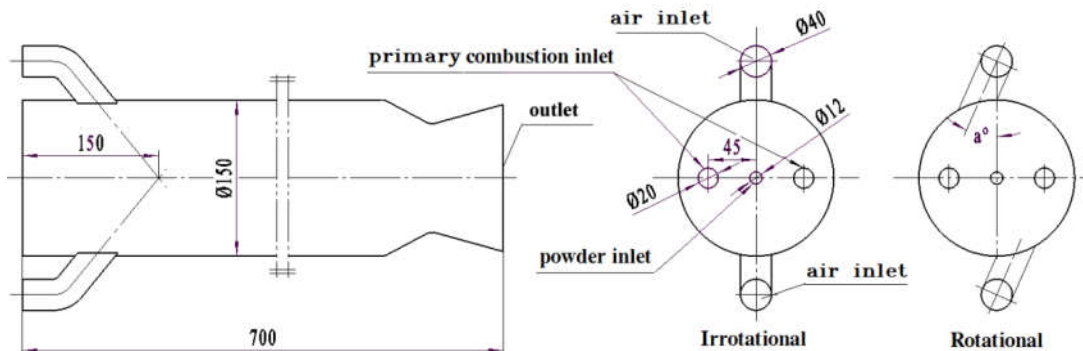


Figure 2 HPSR combustion chamber structure diagram (units are in mm)

Table 1 Tangential inlet angle α

Condition	Different tangential air inlet angle α (°)
Case A	0
Case B	5
Case C	10
Case D	15
Case E	20
Case F	25

2.2 Methods

Reynolds time-averaged N-S equations were solved. The trajectories of particles are traced by the Lagrangian particle trajectory model[1]. The effect of particles on gas phase is considered by adding source term to the gas phase governing equation. Realizable k- ϵ model[2] with swirl modification was used to address turbulence.

The species of HTPB pyrolysis products include CO, H₂, CO₂, H₂O, N₂ mainly and a small amount of HCl, Cl, H, NH₃, HO[3]. To facilitate calculation, it is assumed that the combustion ingredients of fuel-rich HTPB propellant in the combustion gas generator consists of CO, H₂, CO₂, H₂O and N₂. Among them, CO and H₂ will react with oxygen in the air coming from the inlet, and the chemical equation of the combustion reactions as follows,



The gas phase combustion model employs the Eddy-Dissipation Model (EDM)[4]. Boron particles burn in two stages separately, i.e. ignition and combustion stages. The boron particle ignition model is based on the multi-layer oxide structure proposed in literature[5][6]. The total combustion equation for boron particle can be written as:



The boron particle burning rate refers to the literature [7].

The computational domain and grid were generated using the commercial software ICEM[8]. The boundary conditions are shown in the table 2.

Table 2 boundary conditions

Boundary name	Boundary type	Mass flow rate (kg/s)	Gauge pressure (MPa)	Total temperature (K)	Species	Discrete phase
air inlet	mass flow rate	4	0.5	573	22% O ₂ , 78% N ₂	reflect
Primary combustion inlet	mass flow rate	0.26	0.4	1800	45% CO, 20% H ₂ , 10% CO ₂ , 50% H ₂ O, 20% N ₂	reflect
powder inlet	mass flow rate	0.02	0.1	300	N ₂	reflect
outlet	pressure outlet	— —	0.06	255	— —	escape
wall	no slip wall	— —	— —	— —	— —	reflect
Boron particles	Surface injection	0.1	— —	300	B	— —

Figure 3 shows that the oxide layer of boron particles changes with particle trajectory. The ignition distance of case A, B, C, D, E and F are the 185mm, 132mm, 131mm, 163mm, 188mm and 195mm respectively. Figure 4 shows the vorticity distribution within the combustion chamber cross section every 150mm along the axial

direction of the combustion chamber under various cases. Figure 5 shows the mean vorticity of the cross-section of combustion chamber at all cases. Figure 6 shows the temperature distributions of various sections and walls of the combustion chamber. Figure 7 shows the mean temperature of section of the combustion chamber for all the test cases.

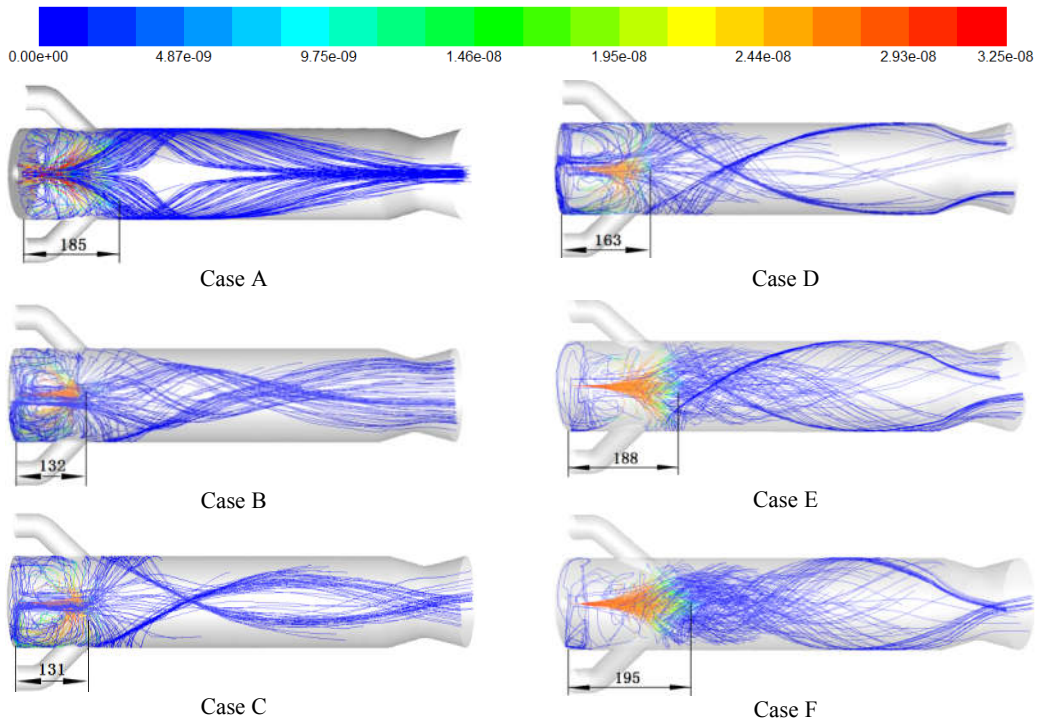


Figure 3 oxide layer of boron particles change with particle trajectory

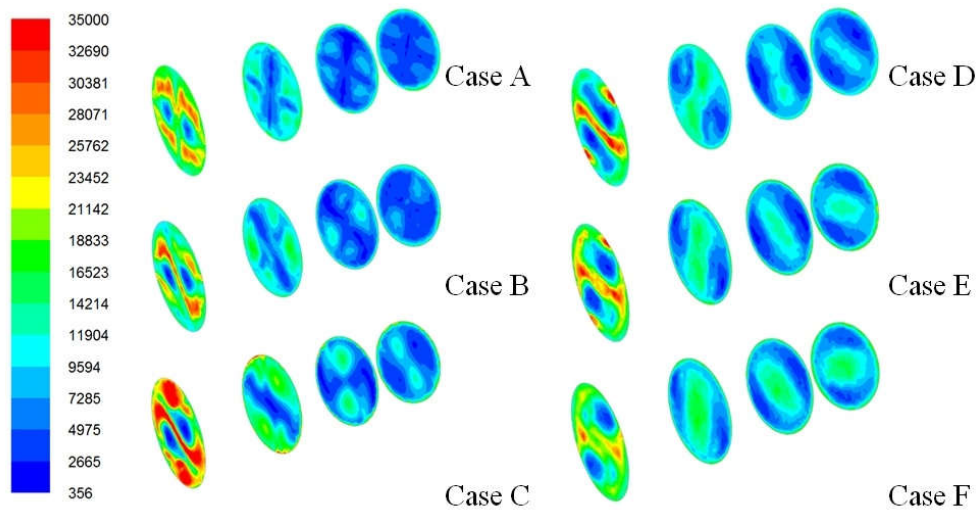


Figure 4 Vorticity distribution in the cross-section of combustion chamber at all cases

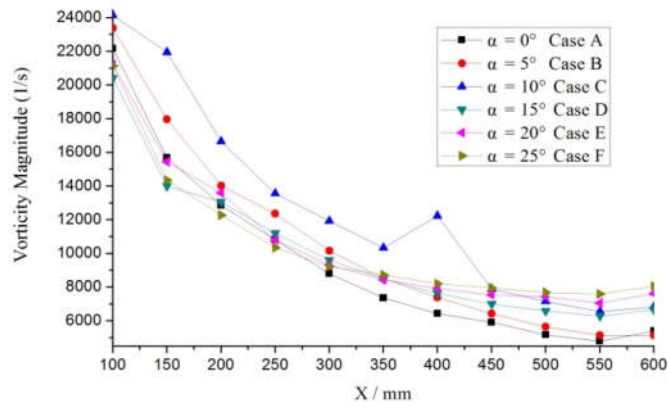


Figure 5 Mean vorticity of the cross-section of combustion chamber at all cases

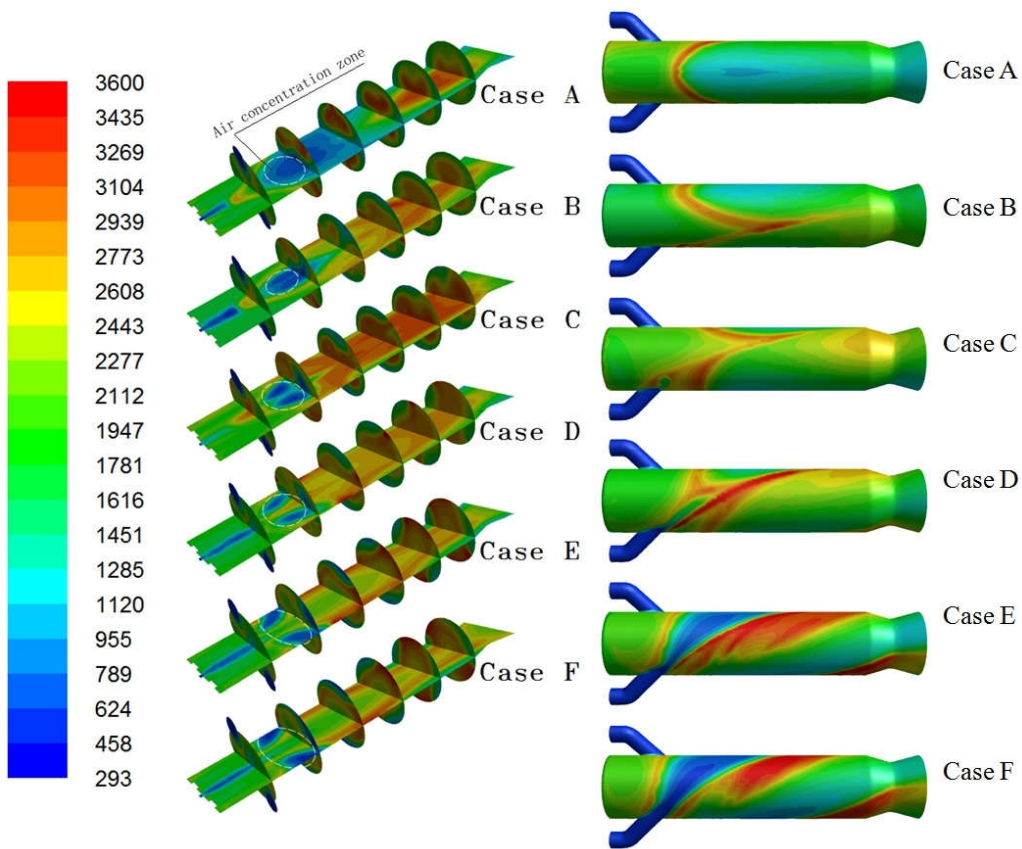


Figure 6 Section and wall temperature distribution of the combustion chamber in all cases

Figure 8 shows the change of combustion efficiency of CO and H₂ along the axial section in combustion chamber under different cases. Figure 9 shows the variation of the combustion efficiency of boron particles along the axial section in the combustion chamber for the different cases examined. Table 3 shows the statistical result of the combustion efficiency in different cases.

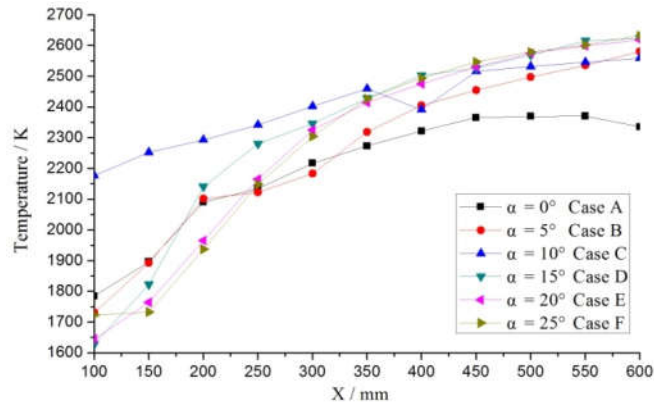


Figure 7 Mean temperature of section of the combustion chamber in all cases

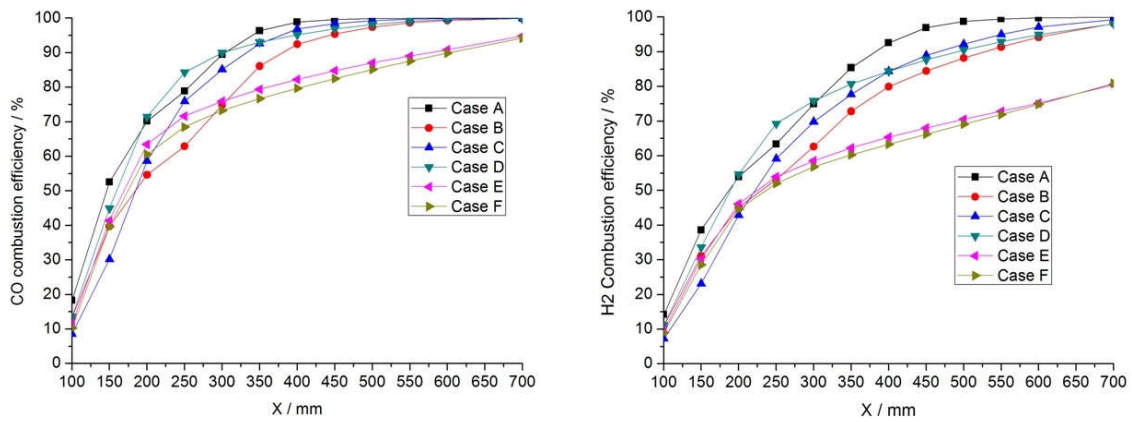


Figure 8 The variation law of CO and H2 combustion efficiency along the axial section

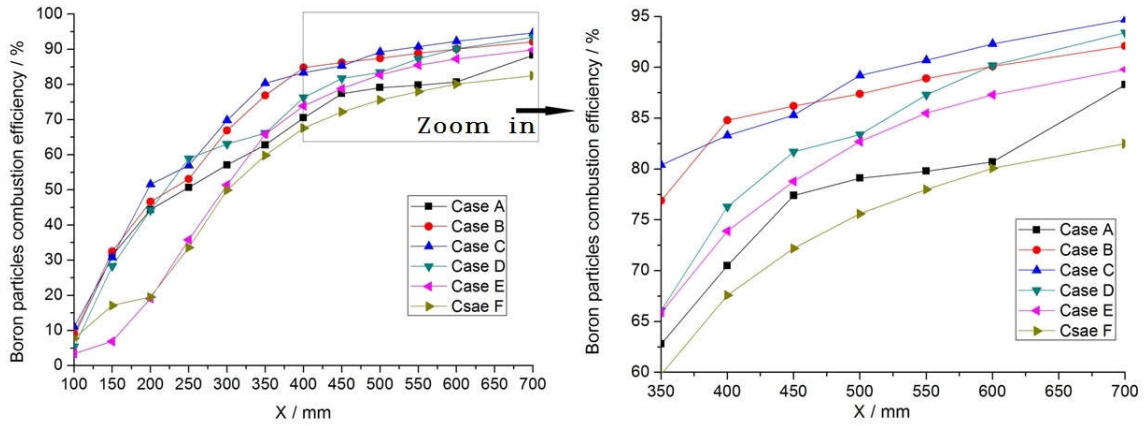


Figure 9 the variation of the combustion efficiency of boron particles along the axial section

Table 3 the combustion efficiency under different cases

Case	CO(%)	H2(%)	Boron Particle (%)	total (%)
A (0°)	99.99	99.94	88.34	92.84
B (5°)	99.84	98.15	92.13	94.57
C (10°)	99.98	99.29	94.76	96.52
D (15°)	99.88	98.08	93.35	95.29

E (20°)	94.80	80.55	89.80	87.06
F (25°)	94.21	80.88	82.51	82.67

Acknowledgements

This work was supported by National Natural Science Foundation of China (No. 51666012)

References

- [1] S. A. Morsi and A. J. Alexander, An Investigation of Particle Trajectories in Two-Phase Flow Systems. *Journal of Fluid Mechanics*. 55 (1972) 193-208.
- [2] T. H. Shih, W. W. Liou, A. Shabbir, Z. Yang, and J. Zhu, A New k- ϵ Eddy-Viscosity Model for High Reynolds Number Turbulent Flows - Model Development and Validation, *Computers Fluids*. 24 (1995) 227–238.
- [3] W. Cai, P. Thakre, V. Yang, A model of AP/HTPB composite propellant combustion in rocket-motor environments, *Combustion Science and Technology*. 180 (2008) 2143–2169.
- [4] B. F. Magnussen and B. H. Hjertager. On mathematical models of turbulent combustion with special emphasis on soot formation and combustion. *Symposium (International) on Combustion*. 16 (1977) 719-729.
- [5] X. Hu, Y. Xu, W. Ao, Z. Zeng, C. Hu, X. Zhu, Ignition model of boron particle based on the change of oxide layer structure, *Proceedings of the Combustion Institute*. 37 (2019) 3033-3044.
- [6] Y. Xu, X. Hu, H. Zou, Y. Li, Z. Zeng, Research on Model of Ignition of Boron Particle Based on Multiple Oxide Layer Structure, *Acta Armamentarii*. 37 (2016) 2242-2250.
- [7] S. C. Li, F. A. Williams, Ignition and combustion of boron in wet and dry atmospheres, *Symposium (International) on Combustion*. 23 (1990) 1147-1154.
- [8] ANSYS Inc., *Ansys ICEM CFD User's Manual*. Canonsburg, PA 15317, 2013.